

A 34-Year Timing Solution of the Redback Millisecond Pulsar Terzan 5A

ALEXANDRA C. ROSENTHAL,^{1,2} SCOTT M. RANSOM,^{2,1} KYLE A. CORCORAN,¹ MEGAN E. DECESAR,³
PAULO C. C. FREIRE,⁴ JASON W. T. HESSELS,^{5,6} MICHAEL J. KEITH,⁷ RYAN S. LYNCH,⁸ ANDREW LYNE,⁷ DAVID J. NICE,⁹
INGRID H. STAIRS,¹⁰ BEN STAPPERS,⁷ JAY STRADER,¹¹ STEPHEN E. THORSETT,¹² AND RYAN URQUHART¹¹

¹University of Virginia, Department of Astronomy, Charlottesville, VA 22904, USA

²National Radio Astronomy Observatory, 520 Edgemont Rd., Charlottesville, VA 22903, USA

³George Mason University, Fairfax, VA 22030, resident at the U.S. Naval Research Laboratory, Washington, D.C. 20375, USA

⁴Max-Planck-Institut für Radioastronomie, Auf dem Hügel 69, D-53121 Bonn, Germany

⁵ASTRON, the Netherlands Institute for Radio Astronomy, Oude Hoogeveensedijk 4, 7991 PD Dwingeloo, The Netherlands

⁶Anton Pannekoek Institute for Astronomy, University of Amsterdam, Science Park 904, 1098 XH, Amsterdam, The Netherlands

⁷Jodrell Bank Centre for Astrophysics, Department of Physics and Astronomy, University of Manchester, Manchester M13 9PL, UK

⁸Green Bank Observatory, PO Box 2, Green Bank, WV 24494, USA

⁹Department of Physics, Lafayette College, Easton, PA, 18042, USA

¹⁰Dept. of Physics and Astronomy, UBC, 6224 Agricultural Road, Vancouver, BC V6T 1Z1 Canada

¹¹Center for Data Intensive and Time Domain Astronomy, Department of Physics and Astronomy,
Michigan State University, East Lansing, MI 48824, USA

¹²Department of Physics, Willamette University, Salem, OR 97301, USA

ABSTRACT

We present a 34-year timing solution of the redback pulsar system Terzan 5A (Ter5A). Ter5A, also known as B1744–24A or J1748–2446A, has a 11.56 ms pulse period, a $\sim 0.1 M_{\odot}$ dwarf companion star, and an orbital period of 1.82 hours. Ter5A displays highly variable eclipses and orbital perturbations. Using new timing techniques, we have determined a phase-connected timing solution for this system over 34 years. This is the longest ever published for a redback pulsar. We find that the pulsar’s spin variability is much larger than most globular cluster pulsars. In fact, of the nine redback pulsars with published or in preparation long-term timing solutions, Ter5A is by far the noisiest. We see no evidence of strong correlations between orbital and spin variability of the pulsar. We also find that long-term astrometric timing measurements are likely too contaminated by this variability to be usable, and therefore require careful short-term timing to determine reasonable positions. Finally, we measure an orbital period contraction of $-2.5(3) \times 10^{-13}$, which is likely dominated by the general relativistic orbital decay of the system. The effects of the orbital variability due to the redback nature of the pulsar are not needed to explain the observed orbital period derivative, but they are constrained to less than $\sim 30\%$ of the observed value.

Keywords: Millisecond Pulsars (1062) — Spider Pulsars, Globular star clusters (656)

1. INTRODUCTION

The high stellar density and resulting high rate of gravitational encounters in globular clusters make them uniquely productive birthplaces for both millisecond pulsars (MSPs) and exotic compact binaries. Globular clusters produce two orders of magnitude more low-mass X-ray binaries per unit mass than the galactic disk

(e.g. Clark 1975; Katz 1975), which results in a similar overproduction of MSPs and exotic systems. To date, 331 pulsars have been identified in 45 globular clusters¹. That number will only increase as pulsar searches with new and more sensitive telescopes continue.

The interactions between pulsars and cluster stars add accelerations to both the pulsar’s spin and orbital parameters (Prager et al. 2017). These effects mean that

Corresponding author: Alexandra C. Rosenthal
acr6tkv@virginia.edu

¹ <https://www3.mpifr-bonn.mpg.de/staff/pfreire/GCpsr.html>

globular cluster pulsars are not useful for certain high-precision timing applications, such as probing the nHz gravitational wave background, but the sheer number of cluster pulsars provides a rich dataset for probing physics such as cluster dynamics (Phinney 1993), cluster gas properties (Abbate et al. 2018; Prager et al. 2017), general relativity (Freire & Wex 2024), and the neutron star equation of state (Lattimer 2021; Özel & Freire 2016).

“Spider” pulsars are one of the exotic and complex types of interacting binaries found in globular clusters. Spider pulsars are a class of MSP with relativistic winds that strongly affect a close companion star. These interesting MSP binaries are so named because ablation from the pulsar wind causes mass-loss indicative of the MSP “eating” its companion. The pulsar’s ablation of its companion creates an ionized wind that delays or completely obscures pulses and perturbs the canonical “perfect” astrophysical clock. This ablated material may approach or fall onto the pulsar, or, more likely, be ejected from the system entirely. It is important to note that this mass transfer mechanism is separate from Roche lobe overflow, even though the irradiation from the pulsar likely helps keep the companion inflated to approximately its Roche lobe radius (Ginzburg & Quataert 2021).

One sub-class of spider pulsars are the redbacks. Redback systems have main sequence companions of mass $M_c \gtrsim 0.1 M_\odot$ (Roberts 2013; Chen et al. 2013). These redback companions are brighter and have larger radii than isolated main-sequence stars of the same spectral type (De Vito et al. 2020). In the galactic field, such a system forms from a binary with a short orbital period and a main sequence companion that filled its Roche lobe. The over-representation of spider pulsars in globular clusters suggests that they may also be produced by dynamical effects that are extremely rare in the Galactic disk. Redback formation is not well understood (see De Vito et al. (2020) for a summary of formation paths), but must involve a significant period of mass transfer (Chen et al. 2013), as redbacks also tend to be the fastest spinning MSPs (and the fastest MSP known is another Ter5 redback, Ter5ad, Hessels et al. 2006). Once a system is visible as a redback, mass transfer isn’t presently occurring (Roberts 2013). Whether redbacks represent a temporary pause in the transitional MSP state, such as that observed in M28I and J1023+0038 (Papitto et al. 2013; Stappers et al. 2014; Patruno et al. 2014) is unclear.

This paper focuses on Ter5A, which is one of the most compact redback systems known and has the shortest orbital period of any redback. It was the second spider

pulsar system discovered, and the first redback system detected (Lyne et al. 1990; Nice et al. 1990), though at the time the distinction between the two classes of spider pulsars had not been established. It is the brightest of the 49 confirmed MSPs in Terzan 5 (Martsen et al. 2022; Padmanabh et al. 2024), and one of the furthest MSPs from the cluster core. The dense cluster introduces higher-order accelerations to the pulsar, which perturb its observed spin rate beyond the standard spin-down over time. Ter5A is a uniquely noisy MSP, with timing residuals on the order of milliseconds over decade timescales. This is two orders of magnitude larger than most other known MSPs (Nice et al. 2000). Ter5A is also unusually *less* recycled than almost all other spider pulsars: most spider pulsars have spin periods under 10 ms, while Ter5A’s period is 11.56 ms (a notable exception is the redback B1718-19, which has a 1.004 s period Lyne et al. 1993).

Ter5A’s companion is a $\sim 0.1 M_\odot$ star in a 1.82 hour compact orbit. The ionized wind blown off the companion eclipses the pulsar, most likely via synchrotron absorption (Polzin et al. 2018). With some assumptions regarding the pulsar’s magnetic moment, the companion’s mass loss rate due to irradiation by the pulsar is $2 \times 10^{-12} M_\odot \text{ yr}^{-1}$ (Shaham 1995), which results in an evaporation timescale of ~ 50 Gyr. Thorsett & Nice (1991) also posit a wind model that does not ablate the companion within a Hubble time. Shaham (1995) predicts that this rate is on the threshold between the conditions for accretion of this ablated wind onto the pulsar and expulsion from the system in absence of accretion. In addition to causing eclipses, interactions between the companion and the pulsar produce orbital variations. Ter5A’s companion also causes many other interesting physical effects on the propagation of the pulsar signal (Bilous et al. 2019; Li et al. 2023).

The eclipse usually occurs around phase 0.25 of the orbit (i.e. superior conjunction). However, the eclipsing behavior of the pulsar is highly variable: some observations have pulses even during phase 0.25, and sometimes the pulsar disappears for hours at a time (Lyne et al. 1990; Nice et al. 1990). Additional eclipse-like disappearances at different orbital phases have also been observed (Bilous et al. 2019). The occasional disappearance is attributed to the system being entirely enshrouded by ablated material. The eclipses are also frequency-dependent: the observing frequency impacts the duration and even the appearance of the eclipse (Nice et al. 1990; You et al. 2018). The eclipses are also longer than expected for a companion confined to its Roche lobe, implying some form of continuous mass loss, whether by Roche lobe overflow, stellar wind, or

irradiation by the pulsar (Nice et al. 2000). Numerical simulations by Tavani & Brookshaw (1993) imply Ter5A’s irregular and long-term eclipses can be generated by a companion mass-loss rate of $4 \times 10^{-13} M_{\odot}/\text{yr}$, which is within a factor of ten of that estimated by Shaham (1995).

The irregular nature of the eclipse, accelerations from the cluster, and effects from Ter5A’s companion have made long-term timing efforts prohibitively difficult. Accounting for the accelerations is a well-documented process (e.g. Prager et al. 2017; Ridolfi et al. 2016), but accounting for the other variations is difficult on long timing baselines because the orbital parameters also change stochastically over time. Without timing methods capable of handling these complications, reback timing has only been attempted on shorter time spans ranging from a few years in length (Archibald et al. 2013; Deneva et al. 2016; Prager et al. 2017; Miraval Zanoni et al. 2018; Ghosh et al. 2024) to a decade (Nice et al. 2000; Ridolfi et al. 2016). Longer timing baselines have exploited new timing techniques to accommodate orbital variations, such as Thongmeearkom et al. (2024)’s 15-year timing solution, which uses Gaussian Process Regression to track orbital evolution in Fermi data. Additionally, timing the system over shorter time spans has been attempted using custom methods to account for the changing orbital parameters (Nice et al. 2000; Bilous et al. 2011).

Using ~ 20 years of archival Green Bank Telescope (GBT) data, ~ 10 years of older Very Large Array (VLA) and Green Bank 140-foot telescope data (Nice et al. 2000), ~ 34 years of data from the Lovell Telescope at Jodrell Bank Observatory (JB) dating from the pulsar’s 1989 discovery to present, four Parkes Radio Telescope (Parkes) observations, the timing programs PINT² (Luo et al. 2021; Susobhanan et al. 2024) and tempo³, and a new piecewise continuous binary timing model (O’Neill et al, in prep), in addition to a new isolation technique that decouples the orbital variability from the timing of the pulsar, we are able to unambiguously track the pulsar spin evolution over 34 years. This is the longest timing solution for a reback system ever produced, and the longest currently possible.

2. OBSERVATIONS

Our timing solution incorporates data from five telescopes: The 100 m Green Bank Telescope (GBT); the Green Bank 140 ft Telescope (GB140); the Very Large Array (VLA); Murriyang, the Parkes Radio Telescope

(Parkes); and the Lovell telescope at Jodrell Bank Observatory (JB).

We started with 244 observations of Ter5A spanning MJDs 47965–60144 (i.e. 1990.2–2023.5) from GBT, GBT140, VLA, and Parkes. The majority of observations were made between MJDs 53193–60144 (i.e. 2004.5–2023.5) with the GBT primarily with the L-band (1.0-1.8 GHz) and S-band (1.6-2.5 GHz) receivers. Over the span of this dataset, the GBT backend processing system changed from SPIGOT (Kaplan et al. 2005) to GUPPI (DuPlain et al. 2008) to VEGAS (Prestage et al. 2015). The SPIGOT observations are described in Ransom et al. (2005). The GUPPI and VEGAS observations are described in Martsen et al. (2022). Data prior to MJD 55422 were processed using incoherent dedispersion, and data after 55422 – most of the GUPPI data and all of the VEGAS data – were processed using coherent dedispersion. We folded subbanded searchmode data, where the original raw data was partially dedispersed to the average DM of the cluster, partially downsampled in time resolution, and had been converted to total intensity, modulo the predicted spin period, and integrated over one-minute intervals to recover the pulse times of arrival (TOAs).

Prior to MJD 53193 (August 2004), most of the TOAs are a combination of VLA 1660 MHz data taken with the Princeton Mark3 backend, GB140 800 MHz and L-band data taken from 1990–1999 with the Spectral Processor, and several early GBT observations between 2000–2004. Details on these older TOAs can be found in Nice et al. (2000); Nice & Thorsett (1992). We incorporate data from Parkes taken in search mode on four days between MJDs 50800–52000 at L-band in several different observing modes. We note that the VLA, GB140, and GBT observations prior to MJD 53193 were available only as pre-calculated TOAs and so were generated slightly differently and using different pulse templates from the later data. Those earlier datasets require systematic timing offsets between themselves and the later GBT data (i.e. JUMPs).

After cleaning and phase-connecting the GBT, GB140, VLA, and Parkes data using the methods outlined in sections 2.1 and 3, we compared our results to JB observations spanning from discovery to June 2024. The JB data consist observations of typically between 12 and 30 minutes duration with the Lovell telescope at L-band and were processed by one or more of three backend systems: 1) an incoherently-dedispersing analogue filterbank (AFB) with a total bandwidth of 32 MHz, spanning MJDs 47952-55196 (1990.2-2020.0) 2) an incoherently dedispersing digital filterbank (DFB) (EPTA Collaboration and InPTA Collaboration et al.

² <https://github.com/nanograv/PINT>

³ <https://tempo.sourceforge.net/>

2023) with a total bandwidth of 384 MHz, spanning MJDs 54973-60490 (2009.0-2024.5) and 3) a coherently-dedispersing system based upon a ROACH processor (EPTA Collaboration and InPTA Collaboration et al. 2023) with a total bandwidth of 400 MHz split into two bands, spanning MJDs 55679-60321 (2011.4-2024.0). The incoherent systems provided TOAs from 3-minute integrations, while the coherent system used 2.5-minute integrations. The JB data was already phase-connected and matched well with our simple timing solution (see Figure 2), and our model accommodating changing orbital parameters (see Figure 3), demonstrating that our novel methodology replicates traditional solutions.

Observation information is tabulated in Table 1. All observations, except JB observations, are band-averaged, and we leave all investigations of short-timescale frequency-dependent timing issues for future work.

2.1. Data Cleaning

Before timing Ter5A, we removed the effects of the eclipse from observations because the time-variable ionized gas can cause unpredictable time delays in the measured pulses. To remove most of these effects, we cut all TOAs corresponding to an orbital phase between 0.0 and 0.5, where the pulsar was most likely to be eclipsed. We further manually inspected the data to remove any remaining large-scale effects of the eclipse. A summary of the phase-cleaned observations is presented in Table 1.

Figure 1 shows an example of what eclipses look like in the timing data and what the timing residuals look like after cleaning TOAs. As the pulsar moves behind a clump of ionized gas, this gas increases the effective dispersion measure (DM), causing pulse delays. The stochastic variability of the wind from the companion makes timing delays unpredictable. While every orbit has some eclipse around phase 0.25, the width and effect of this eclipse varies significantly between observations. Several observations show additional micro-eclipses or hours-long total disappearances. This is one reason that long-term timing of this system was previously prohibitively difficult.

3. TIMING METHODOLOGY

Timing this system required new methodologies. The main reason that redback systems are difficult to time over long baselines is because the variable gas interactions and complicated companion effects cause random orbital period variations. These effects mean that timing solutions do not maintain phase coherence for more than a few years, or even a few months, beyond the end of any given timing solution. Phase-connection, which

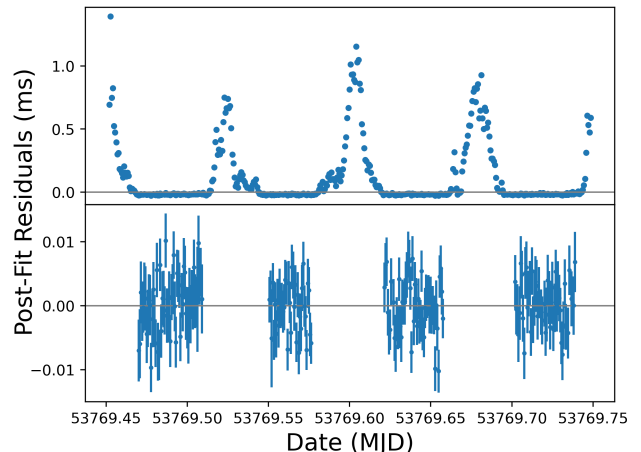


Figure 1. Timing residuals from a representative day (MJD 53769) before (top) and after (bottom) removing the effects of the eclipses. These data span four orbits. Note the vertical scales differ in the panels – cleaning the eclipse reduces the residuals by two orders of magnitude. The eclipses are not perfectly symmetrical or identical from orbit to orbit. This reflects the rapidly-changing gas environment.

means successfully tracking every rotation of the pulsar, is the first step in generating a timing solution.

We measure orbital variations with the parameter “T0.” T0 is the precise time of the periastron of the orbit. For an effectively circular system such as this one, where eccentricity is set at zero, T0 is defined as the time of the ascending node, which is the instant when the pulsar crosses the plane of the sky moving away from the observer. For well-behaved binary systems, this value evolves uniformly over time according to Eqn 1 (see section 4.3), but for redback systems, interaction with the companion drives orbital wander that results in unpredictable time-variable T0s. As a result, standard pulsar timing cannot easily account for this orbital behavior, which limits the duration that redback pulsars can maintain phase coherence. Most earlier spider pulsar timing used the so-called BTX timing model, which uses many terms in a Taylor expansion of the orbital frequency to account for this orbital wander. Such expansions can be highly numerically unstable and extremely poorly extrapolate orbital phase. This exacerbates redback timing difficulties. In this paper we outline two different and effectively new methods (see sections 3.2 and 3.3) by which we successfully timed Ter5A.

3.1. Generating TOAs

Table 1. Summary of observational data.

Observatory	Num. Observations	Num. TOAs	Frequency (MHz)	Median Error (μ s)	Dates (MJD)
GBT	52	6279	820–2000	4.43	52466–55137
GBT*	61	6477	820–2165	4.31	55422–60144
Green Bank 140 ft	91	1073	670–1600	23.7	47966–15363
Parkes	4	629	1316–1454	24.3	50800–52000
VLA	36	699	1667	11.1	48190–50975
Jodrell Bank	219	1481	1396–1640	31.4	47952–60491
Jodrell Bank*	68	730	1414–1725	15.6	55679–60321

*Indicates data uses coherent de-dispersion. All other data are incoherently de-dispersed.

We searched each observation of the GBT and Parkes data for pulsations using the `spider_twister`⁴ package, which searches over orbital phase by performing trial folds to determine a most probable T0. With an adequate local orbit, we then re-folded the observations with one minute integrations to determine TOAs, which could then be used to determine a much more precise T0 via timing software (e.g. `Tempo` or `PINT`). For the GBT data, the folding and TOA determination were performed with the `prepfold` and `get_TOAs.py` commands, respectively, from `PRESTO`⁵ (Ransom 2001, 2011).

While this produced good starting parameters for individual days, we needed to use a model that accommodated time-varying T0s to determine a long-term timing solution. We independently used two different techniques to determine the same long-term timing solution.

3.2. Piecewise Method

Using `PINT`, we fit long-term timing parameters through a bootstrapping process, starting with initial parameters from published solutions (spin frequency, frequency derivative, position, DM, orbital period, and semimajor axis; e.g. Nice et al. 1990; Nice et al. 2000; Urquhart et al. 2020), and phase-connecting the pulsar in 2–3 year segments.

We followed a four-step phase-connection process. First, we determined orbital phases (i.e. the best T0) for each observation (see section 3.1). Second, we phase-connected overlapping two-year chunks of data, fitting for frequency, first and second frequency derivatives, and position. Third, we verified that the number of pulse rotations between each TOA in the overlapping sections were identical for each phase-connected section. Fourth, we joined all the sections together using the rotational counts between all the TOAs.

This process produced a phase-connected timing solution. We next held the T0 values fixed while fitting for

long-term parameters: orbital period, spin frequency, spin frequency derivatives one through five, DM, and DM derivative. `PINT` struggled with fitting the 10000+ TOAs with the `binary_piecewise` model, given the large number of free parameters, which is one of the reasons we pursued an additional “isolation” fitting technique (see section 3.3). To accommodate non-GBT data, we manually fit for the JUMPs between datasets. We did this by fixing all long-term parameters and then isolating portions of the data that had two different instruments and fitting for JUMPs in these isolated portions in a pair-wise round-robin fashion until instrumental offsets were smaller than offsets due to T0 measurement errors and much smaller than overall timing noise.

In order to nail down the short-term orbital variations within the long-term solution, we assumed that the orbital period was constant over roughly two to four-week periods, and used multiple observations within such periods to constrain the piecewise constant T0 for those data. This was more important for the data before the year 2000, which had fewer and less precise TOAs.

The orbital phase residuals between the measured and predicted T0s, assuming a constant orbital period (see sections 4.3 and 4.4), showed a stochastic-like pattern with a general quadratic trend. We used a least-squares fit to determine a best-fit orbital period derivative from the T0s, and also performed a Gaussian Process Regression which allowed us to predict and refine T0 measurements that were poorly determined in the first iteration.

The result is a phase-connected timing solution with relatively well-behaved TOAs in individual observations and relatively smooth long-term behavior, as well as a time series of orbital phase wander as determined by the measured values of T0 (Figures 3 and 5).

3.3. Isolation Technique

Besides this piecewise technique, and as part of a related project on long-term timing of other globular cluster redbacks (Corcoran et al, in prep), we also phase-connected the system without breaking it into chunks by removing the effects of the binary and effectively “iso-

⁴ https://github.com/alex88ridolfi/SPIDER_TWISTER

⁵ <https://github.com/scottransom/presto>

lating” the pulsar. We used PINT and the accurately known T0 values measured over short timescales (see Table 4), and the long-term P_{orb} , and \dot{P}_{orb} values to subtract off the Roemer delays from the binary orbit from the TOAs for each observation, resulting in a much simpler dataset: an “isolated” pulsar with far fewer parameters to fit.

This isolation technique effectively de-couples the orbital variations from the long-term spin behavior of the pulsar. Since the arrival times are topocentric (i.e. in the reference frame of the observatories), but the binary Roemer delays need to be computed in the barycentric frame, we had to perform a first-order correction to the predicted Roemer delays to compensate for the difference in those frames. We tested this technique with simulated binary TOAs and were able to remove all orbital effects to better than 100 ns. It is likely to be useful in other long-term redback timing efforts, and can be implemented in PINT with just a few lines of code.

Ultimately we used the short-term timing position measured with the GBT Spigot data (see Figure 8 and Table 3) rather than a long-term timing-fitted position in our final model, and *Gaia*-measured proper motion values (Vasiliev & Baumgardt 2021) for the cluster rather than the timing-fitted proper motion of Ter5A (see section 4.5). The long-term timing parameters are presented in Table 5.

4. RESULTS

4.1. Simplest Long-Term Model

If we use the obtained pulse numbers but do not accommodate for changing T0, and fit for spin frequency, and the first and second spin frequency derivatives, we do obtain a phase-connected timing solution with a smooth overall trend, but within any individual observation the pulse phase varies by 5–10%. This solution is shown in Figure 2 and in Table 5.

4.2. Spin Frequency Derivatives

We fit the data through five spin frequency derivatives to show the extent of the un-modeled spin-noise present in the data. Figure 3 shows the evolution of fit with successive derivatives. All plots shown have been fit for DM, DM derivative, frequency, and the number of frequency derivatives indicated.

Ter5A is a complex system and over a 34-year timespan the DM changes significantly. As a result, the DM is not well fit for much of the dataset. However, compared to the timing noise systematics, the variations due to the DM are small (i.e. few percent of a rotation for the F1-based solution and up to $\sim 10\%$ of a rotation for the F5-based solution) and not prohibitive to find-

ing a timing solution. In principle, we could fit for the DM on each observation, but simultaneously fitting for ~ 300 additional free parameters becomes computationally difficult, and in addition, on many days the DM changes significantly on minute to hour timescales. We acknowledge this issue and leave it for future work.

There is an apparent abrupt timing feature around the year 2000 (i.e. MJD 51700). This is noted in Nice et al. (2000) and corroborated by our observations. While it is unfortunate that this feature occurs during the least-well sampled period of our data, the unambiguous phase connection of the Parkes and Jodrell Bank observations during that time period suggests this feature is real and corresponds to some physical change in the system. We note that whatever this physical change is, it appears strongly only once the second frequency derivative has been subtracted. We also note that several other timing features of smaller amplitude appear later in the data (e.g. around MJDs 55000, 56000, and 58000).

We measure a spin frequency derivative (i.e. F1) of $\sim 1.35 \times 10^{-16} \text{ Hz s}^{-1}$, depending on the exact spin model used. This positive value is consistent with other measured values (e.g. Lyne et al. 1990; Nice & Thorsett 1992; Prager et al. 2017). The intrinsic spin-down rate of the pulsar must be negative. The positive measured first spin derivative value is likely due to the globular cluster accelerating the pulsar toward the observer from the far side of the cluster. There are additional mechanisms that contribute to apparent positive F1 values, and they usually affect the orbit and spin equally. We discuss this in the next two sections.

From Figure 3, it is clear that spin variations are not correlated with orbital variations. X-ray activity also does not appear to correlate with either of these variations, nor do the days in which the pulsar was undetected in radio observations.

The total fractional sensitivity of the pulsar’s spin (median spin phase error divided by the total pulse phase covered by the dataset, $T \times F0$) is 4.4×10^{-15} while the total fractional sensitivity of the pulsar’s orbit (median T0 phase error divided by the total orbital phase covered by the dataset, $T \times P_{\text{orb}}^{-1}$) is 9.3×10^{-11} , so the spin residuals are substantially more sensitive to torques and other effects on the system than the T0 residuals.

We examine the spectrum of the spin residuals by taking a Fourier decomposition of the F0–F1 solution (Figure 3, top panel) using a single “median residual” TOA from each observation. We calculated the powers of the components using the `get_wavex_amps()` and `get_wavex_freqs()` functions of `pint.utils` and determined a best-fit line using `scipy.curve_fit()`. This gives a steep power-law-like spectrum with a spectral

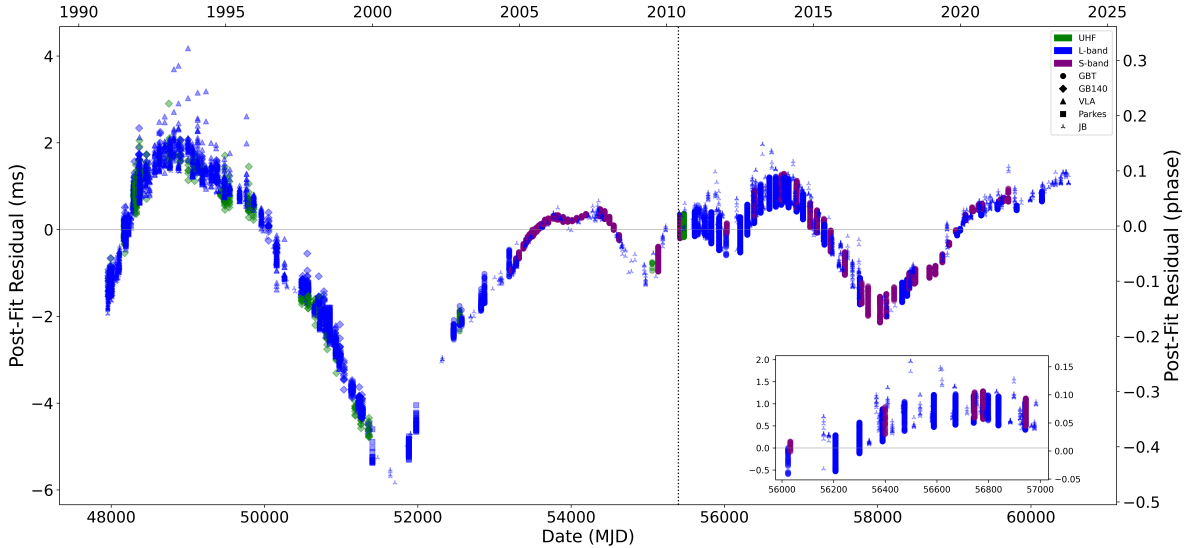


Figure 2. The long-term timing solution for Ter5A for a constant T_0 . The vertical dotted line represents where the processed TOAs switched from incoherent to coherent de-dispersion. For readability, only every tenth TOA is plotted. Note that the long-term behavior is smooth and phase-connected, while observations further from the center, which have less precise T_0 values, show larger and larger systematics from errors in the predicted orbital phase. The inset is a zoom-in that clearly shows the spread of TOAs over individual observations and short-term variations.

index of $-5.54(7)$, as shown in Figure 4. The error represents the span between the maximum and minimum slope values estimated by multi-variate gaussian sampling using the fit covariance matrix. The first two harmonics are the most significant and dominate the measured spectral index.

4.3. Orbital Variations

In the absence of external effects, such as that of accelerations from the globular cluster, tidal effects in the bloated companion star, gravitational wave radiation from the compact orbit, and mass transfer or loss from the companion, we can expect T_0 will evolve according to

$$T_0_n = T_0 + n \times P_{\text{orb}}, \quad (1)$$

where T_0 is some reference measured T_0 , n is an integer number of orbits that have elapsed between T_0 and T_0_n , and P_{orb} is the orbital period of the binary (1.82 hours). When we compare our measured T_0 values with those predicted by this equation using a precise estimate for P_{orb} (see Table 5), we find that the measured values vary across ~ 10 seconds, as shown in Figure 5. There is an apparent quadratic trend corresponding to an orbital period derivative (\dot{P}_{orb}). Adjusting for the effects of \dot{P}_{orb} , as described in the next section, results in a random process varying across ~ 5 seconds, also shown in Figure 5.

We also performed a Gaussian Process Regression on the measured T_0 values (see Figure 5) to estimate how smooth the variations might be in time and to better estimate T_0 values on days where it could not be measured well. On several days, micro-eclipses or significant ionized gas effects during the observation cause strong systematic offsets in the T_0 measurements due to unmodeled DM changes. Our final values are presented in Table 4.

We determined the Power Spectral Density (PSD) (see Figure 6) of these \dot{P}_{orb} subtracted orbital variations by using `scipy.curve_fit()` to take a best fit line of the portion of the PSD between the first bin ($8.0 \times 10^{-5} \text{ d}^{-1}$) and where the spectrum turns into white noise (10^{-3} d^{-1}). The first bin is partially covariant with \dot{P}_{orb} and therefore has a reduced power. This produces a power-law with a spectral index γ of $-0.9(2)$.

Three other works have assessed the spectral index of T_0 variations in redbacks. From an analysis of Fermi-LAT observations of three redback pulsars, [Thongmeearkom et al. \(2024\)](#) found orbital phase wander spectral indices constrained to $\gamma < -2.4$, $\gamma = -3.81^{+0.32}_{-0.48}$, and $\gamma < -5.4$. [Corcoran et al. \(in prep\)](#) surveys five redbacks and measures spectral indices of $\gamma = -0.7(2)$, $-0.7(2)$, $-0.9(1)$, $-1.1(2)$, and $-1.7(2)$. [Clark et al. \(2021\)](#)'s analysis concluded there were too few significant frequency bins for a meaningful measurement. Our measurement of $\gamma = -0.9(2)$ is shallower than the in-

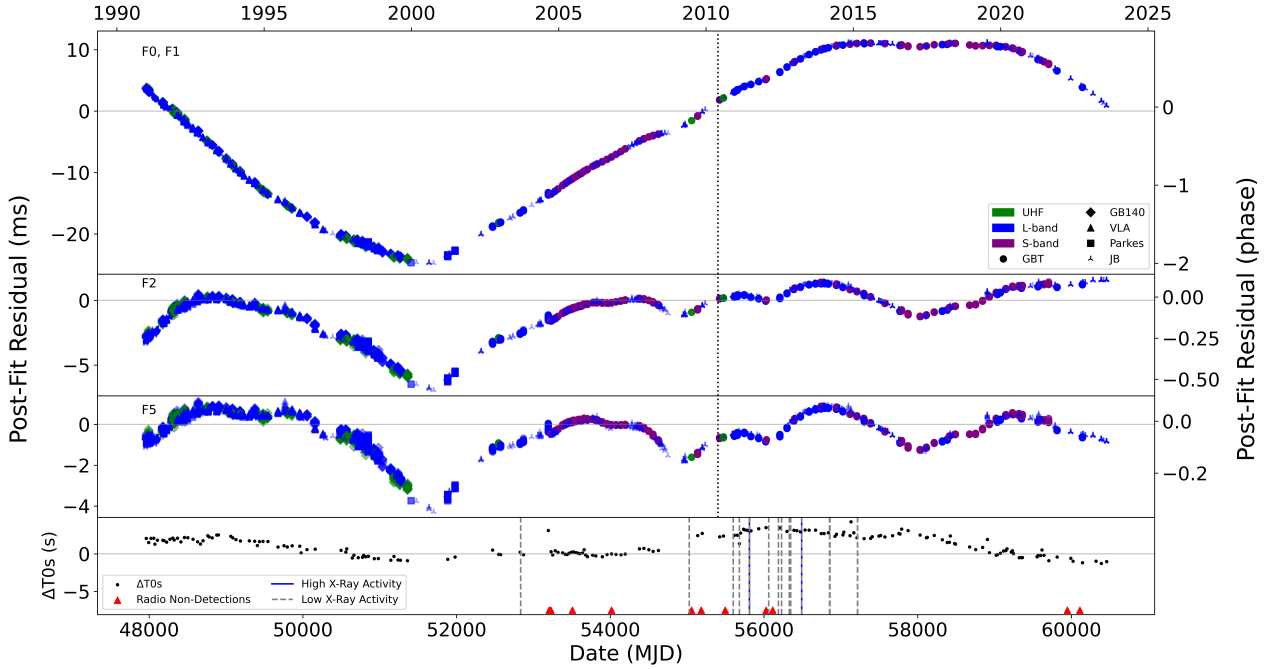


Figure 3. The top three panels show the timing residuals of three different Ter5A spin frequency derivative fits (i.e. F0–F1, F0–F2, and F0–F5, as indicated in the upper left hand corner of each panel). The bottommost panel shows orbital variations ΔT_0 with \dot{P}_{orb} removed (see sections 4.3 and 4.4 for more details) as well as X-ray detections (see section 4.6) and radio non-detections. The vertical dotted line represents where the processed TOAs switched from incoherent to coherent de-dispersion. For readability, only every tenth TOA is plotted. Note the decreasing range covered by the y-axes in each case, showing nominally better fits. Strong systematic trends still remain in the residuals. There also remain strong DM and system JUMP effects, most evident in the data prior to the year 2000, which could be addressed in future work. It is apparent that X-ray activity, radio non-detections, orbital variations, and spin variations are not strongly correlated with each other.

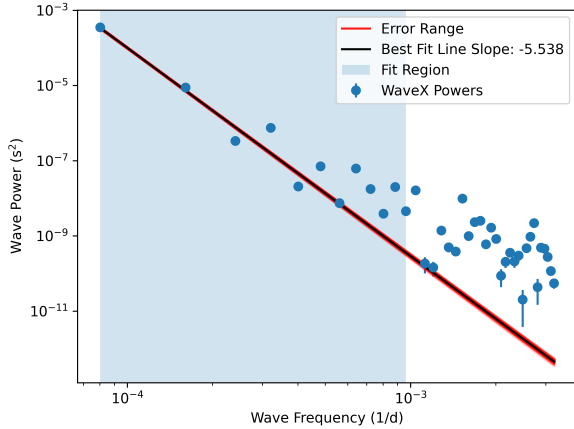


Figure 4. Fourier component analysis of spin residual variations with F0 and F1 subtracted out (see Figure 3, top panel). The error band was estimated by multi-variate gaussian sampling using the fit covariance matrix.

indices observed in Thongmeearkom et al. (2024) and consistent with those observed in Corcoran et al. (in prep).

We compare our results to the Applegate model (Applegate 1992), which predicts that spider pulsar systems should show periodic modulations in orbital period due to cycles of magnetic activity and changing quadrupole moment of the companion star. We see no evidence for such periodicity on the scale of up to ~ 20 years.

4.4. Orbital Period Derivative

The orbital period change due to gravitational wave emission (Peters & Mathews 1963) can be expressed as a function of the component masses m_1 and m_2 and the well-known orbital parameters (e.g., Taylor & Weisberg 1982; Freire & Wex 2024):

$$\dot{P}_{\text{orb}} = -\frac{192\pi}{5} \left(\frac{P_{\text{orb}}}{2\pi}\right)^{-5/3} \left(1 + \frac{73}{24}e^2 + \frac{37}{96}e^4\right) \times (1 - e^2)^{-7/2} T_{\odot}^{5/3} m_1 m_2 M^{-1/3}, \quad (2)$$

where e is the eccentricity, P_{orb} is the orbital period, M is the total mass of the system, and $T_{\odot} \equiv GM_{\odot}/c^3 = 4.925490947 \mu\text{s}$. For Ter5A, the eccentricity is zero, sim-

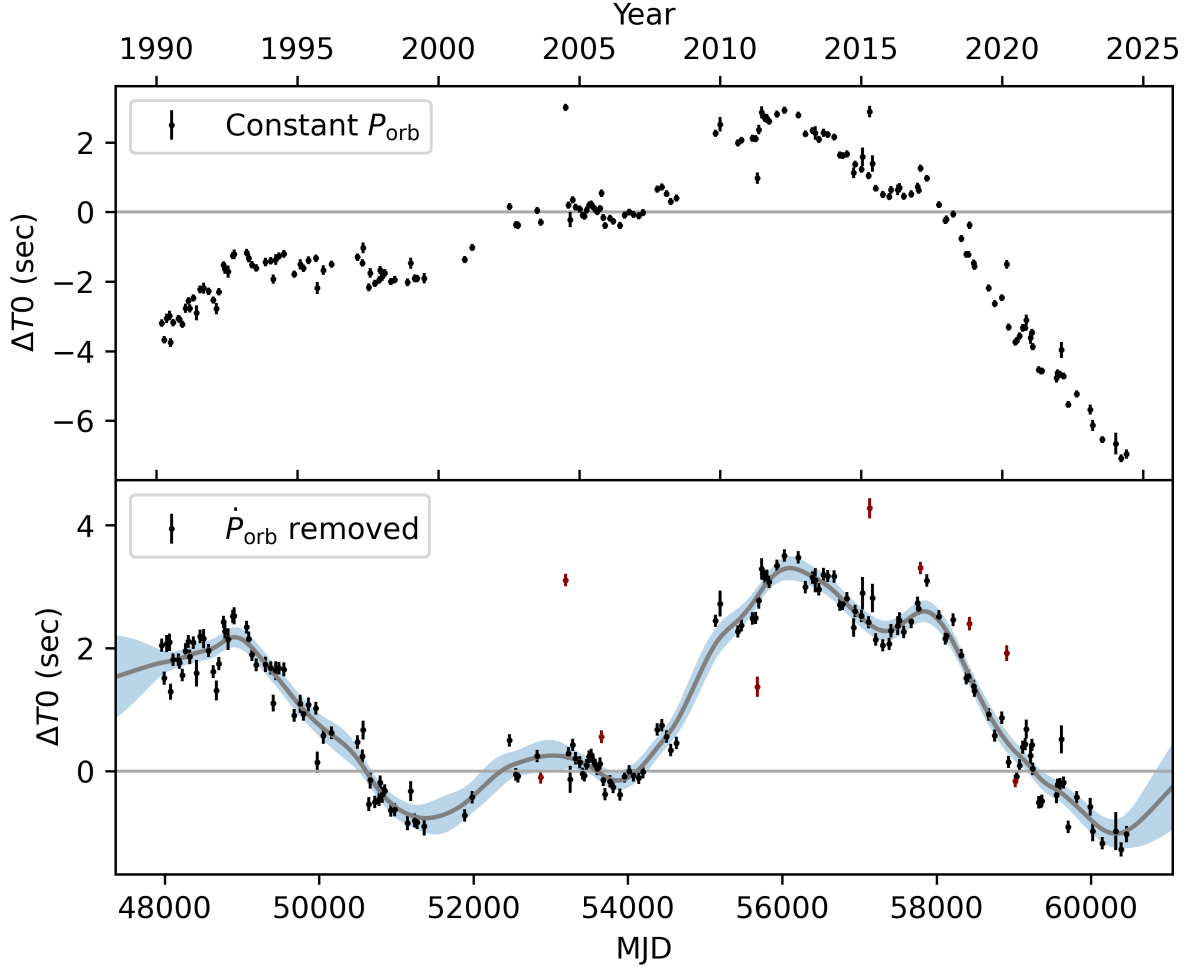


Figure 5. Time of ascending node deviations (ΔT_0) over time for Ter5A assuming a constant orbital period (top) and with the best-fit \dot{P}_{orb} removed (bottom). The bottom panel shows a Gaussian process regression to the measured ΔT_0 values. Red data points are days in which the eclipse effects are covariant with T0 and prohibit accurate measurement, and are excluded from the GPR fit.

plifying Eqn 2 to

$$\dot{P}_{\text{orb}} = -\frac{192\pi}{5} \left(\frac{P_{\text{orb}}}{2\pi}\right)^{-5/3} T_{\odot}^{5/3} m_1 m_2 M^{-1/3}. \quad (3)$$

The observed pulsar spin-down to spin period ratio $(\dot{P}/P)_{\text{obs}}$ can be converted to an acceleration:

$$A_{\text{obs}} = c \left(\dot{P}/P\right)_{\text{obs}}. \quad (4)$$

A_{obs} is the sum of several accelerations:

$$A_{\text{obs}} = A_{\text{int}} + A_{\text{Shk}} + A_{\text{GC}} + A_{\text{gal}}, \quad (5)$$

where $A_{\text{int}} = c \left(\dot{P}/P\right)_{\text{int}}$ is the intrinsic spin-down rate of the pulsar, A_{GC} is the contribution due to acceleration of the pulsar by the globular cluster, and A_{gal} is the contribution due to the acceleration of the pulsar by the

Galactic gravitational potential. A_{Shk} is the apparent acceleration due to the Shklovskii effect which is given by

$$A_{\text{Shk}} = \mu^2 d \quad (6)$$

where μ is the proper motion of the pulsar and d is the distance to the pulsar. Of these, A_{GC} is the dominant term since the pulsar is observed to have a positive frequency derivative.

Orbital period accelerations follow a similar form to Eqn. 5:

$$A_{\text{orb,meas}} = A_{\text{Shk}} + A_{\text{GC}} + A_{\text{gal}} + A_{\text{GR}} + A_{\text{RB}}. \quad (7)$$

$A_{\text{orb,meas}} = c \times \left(\dot{P}_{\text{orb}}/P_{\text{orb}}\right)_{\text{meas}}$ is the observed orbital acceleration. A_{GR} is an acceleration-like term representing the quantity $c \times \left(\dot{P}_{\text{orb}}/P_{\text{orb}}\right)_{\text{GR}}$, the GR-predicted contraction due to gravitational wave emission. A_{RB} is

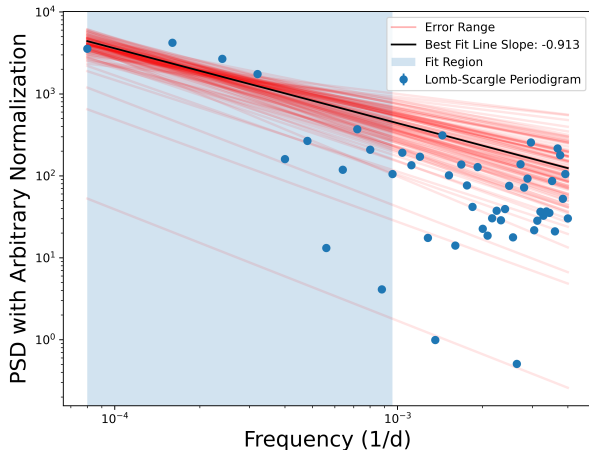


Figure 6. PSD of T0 variations (excluding outliers; see Figure 5) with \dot{P}_{orb} removed. Because \dot{P}_{orb} is quadratic and therefore partially covariant with a single sinusoid, the first bin is likely an underestimate of the true power. The steep-spectrum, as well as the oscillations dominating Figure 5, demonstrate that the signal is dominated by a red-noise process. The error band was estimated by multi-variate gaussian sampling using the fit covariance matrix.

the apparent acceleration due to variations in the companion in the redback system. A_{RB} is not directly measurable, but can be constrained by the span of reasonable A_{GR} values, in combination with the estimates of the other acceleration parameters.

By combining Eqns 5 and 7, we can eliminate the dependency on A_{gal} , A_{GC} , and A_{Shk} (for a breakdown of the predicted contributions of these terms, see Table 2):

$$A_{\text{obs}} - A_{\text{orb, meas}} = A_{\text{int}} - A_{\text{GR}} - A_{\text{RB}}. \quad (8)$$

The quantity $A_{\text{obs}} = c \left(\frac{\dot{P}}{P} \right)_{\text{obs}}$ has a 7% fractional error ($-4.62(34) \times 10^{-10} \text{ m s}^{-2}$) purely due to measurement uncertainty. From fitting linear (i.e. P_{orb}) and quadratic (i.e. \dot{P}_{orb}) terms to the raw T0 residuals (Figure 5, top) we measure $\dot{P}_{\text{orb}} = -2.5(3) \times 10^{-13}$.

Assuming a reasonable age for the pulsar of 5.0×10^9 yr, within a factor of ten, and a surface magnetic field strength B of 8×10^8 G based on the mean of the 16 closest-period pulsars in the ATNF catalogue⁶, excluding globular cluster pulsars, we can predict $\left(\frac{\dot{P}}{P} \right)_{\text{int}}$. Varying B across a reasonable range of 6×10^8 to 10^9 G, we find $\left(\frac{\dot{P}}{P} \right)_{\text{int}} = 4.7_{-2.0}^{+2.6} \times 10^{-18}$, resulting in an intrinsic acceleration of $A_{\text{int}} = 14.0_{-6.0}^{+7.8} \times 10^{-10} \text{ m s}^{-2}$.

⁶ <https://www.atnf.csiro.au/research/pulsar/psrcat/>

A $1.5 M_{\odot}$ pulsar with a $0.09 M_{\odot}$ companion star are reasonable estimates for the masses of the system components. MSPs are typically more massive than canonical pulsars, and the system is highly likely to have a large inclination due to the strong eclipses, meaning $0.09 M_{\odot}$ is a likely companion mass. This yields the prediction shown in Table 2 for a predicted \dot{P}_{orb} of $-2.34_{-0.17}^{+0.22} \times 10^{-13}$, which is consistent with our measured value of $-2.5(3) \times 10^{-13}$. The error range on the predicted value comes from the range of likely surface magnetic field strengths and galactic accelerations.

Strader et al. (2019) measured the masses of 10 redbacks and redback candidates, finding an average mass for redback neutron stars of $1.78 \pm 0.09 M_{\odot}$ with a dispersion of $\sigma = 0.21 \pm 0.09 M_{\odot}$. We therefore examine the viability of a $1.8 M_{\odot}$ pulsar. A $1.8 M_{\odot}$ pulsar with a $0.09 M_{\odot}$ companion predicts a \dot{P}_{orb} of $-2.59_{-0.24}^{+0.17} \times 10^{-13}$, consistent with our measured value of $-2.5(3) \times 10^{-13}$. For the lowest reasonable values of magnetic field and galactic acceleration, a 1.9 – $2.0 M_{\odot}$ pulsar is still consistent with our measured value of \dot{P}_{orb} . Although this higher mass pulsar cannot be definitively ruled out, it seems unlikely that it could have reached this mass while only being spun up to an 11.56 ms pulse period.

We therefore cannot make strong constraints on Ter5A’s mass; it is most likely in the range of 1.5 – $1.8 M_{\odot}$. As a less-recycled redback, it is likely also a less massive one. If we do indeed have a minimum-likely-mass system, the contribution of \dot{P}_{RB} is no greater in magnitude than -6×10^{-14} , but we do not need any \dot{P}_{RB} to explain our results. We conclude that \dot{P}_{orb} is dominated by gravitational wave radiation.

We note that the time for a binary to coalesce due to GR is given by (e.g., Shapiro & Teukolsky 1983):

$$t = \frac{5}{256} \frac{G^3}{c^5} \frac{r^4}{m_1 m_2 (m_1 + m_2)}, \quad (9)$$

where r is the total separation between the two objects. For Ter5A, if the companion was a compact star that would lose no mass, the coalescence time would be ~ 250 Myr. In reality, though, the companion is not compact and more complex binary interactions would occur as the orbit shrinks, dramatically changing this GR-driven evolution.

We also note that we do not expect a measurable value of the contraction of the semimajor axis in timing residuals due to the contraction of the orbit from gravitational wave emission. Over the time period of our observations, \dot{P}_{orb} predicts a change in period that, via Kepler’s third law, corresponds to a fractional change of 2.3×10^{-8} . The fractional error of our timing semi-major axis mea-

Component	Value
$A_{\text{spin,meas}}$	$-4.62 \times 10^{-10} \text{ m s}^{-2}$
$A_{\text{spin,int}}$	$14.00 \times 10^{-10} \text{ m s}^{-2}$
A_{gal}	$3.39 \times 10^{-10} \text{ m s}^{-2}$
A_{Shk}	$1.41 \times 10^{-10} \text{ m s}^{-2}$
A_{GC}	$-21.52 \times 10^{-10} \text{ m s}^{-2}$
A_{GR}	$-85.47 \times 10^{-10} \text{ m s}^{-2}$
$A_{\text{orb,meas}}$	$-110.9(18.0) \times 10^{-10} \text{ m s}^{-2}$
Predicted \dot{P}_{orb}	$-2.34^{+0.22}_{-0.17} \times 10^{-13}$
Measured \dot{P}_{orb}	$-2.5(3) \times 10^{-13}$

Table 2. Predicted contribution of different accelerations to orbital period derivative. The listed value of $A_{\text{spin,int}}$ presumes a magnetic field of $8.0 \times 10^8 \text{ G}$, which is the center of the reasonable distribution. The listed value of A_{gal} is precise to a factor of two (Pathak & Bagchi 2018). Assuming a distance to the pulsar of 6.6 kpc with a $\sim 10\%$ error and the proper motion of the entire cluster 5.61(7) mas/yr (Vasiliev & Baumgardt 2021) yields a value of $A_{\text{Shk}} = 1.41(15) \times 10^{-10} \text{ m s}^{-2}$. A_{GC} is calculated from these values. The listed value of A_{GR} assumes a $1.5 M_{\odot}$ pulsar with a $0.09 M_{\odot}$ companion. Errors on other components are discussed in depth in section 4.4.

surement is 6.4×10^{-6} , so the change in semimajor axis is significantly smaller than our errors and is currently undetectable via timing.

In theory, the relativistic precession of the system (i.e., Susobhanan et al. 2018), predicted to be $\sim 20^{\circ}/\text{yr}$, should be easily measurable. However, in practice, the eccentricity is so close to zero that this is not possible — the precession is entirely covariant with the orbital period.

4.5. Position and Proper Motion

Fitting for position over the entire dataset yields a value that is entirely inconsistent with VLA imaging positions and prior timing-based positions. The source of this discrepancy is two sided. Eclipse variability during long integrations can cause systematic positional offsets in VLA imaging (for further discussion of positional uncertainties, see Fruchter & Goss 2000). On the other hand, long-term pulsar timing systematics also produce massive uncertainties and can strongly affect the position signal in the timing data. However, fitting for position over just 2-3 years of data at a time produces reasonable positions that are both self-consistent and consistent with the proper motion measured by *Gaia* (Vasiliev & Baumgardt 2021). While we cannot get extremely precise positions with this method, short-term timing is good enough to allow multi-wavelength follow-ups, with the caveat that Ter5A’s very low ecliptic latitude ($\beta = -1.4^{\circ}$) means declination measurements via timing are highly imprecise.

Fitting for proper motion over the entire dataset likewise produces nonsensical results; again, long-term timing systematics skew the proper motion measurements. Timing over the entire dataset measures a proper motion in the RA direction of $-1.53(11) \text{ mas/yr}$ and in the Dec direction of $-24.5(3.2) \text{ mas/yr}$. The dispersion in the proper motion of Terzan 5 stars is $\sim 0.5 \text{ mas/yr}$ (Taylor et al. 2022; Gaia Collaboration et al. 2021), so while the RA-proper motion is plausible in comparison with *Gaia*-measured values ($-1.53(11) \text{ mas/yr}$ compared to $-1.989(68) \text{ mas/yr}$) (Vasiliev & Baumgardt 2021), the declination-proper motion radically differs ($-24.5(3.2) \text{ mas/yr}$ compared to $-5.243(66) \text{ mas/yr}$). The source of this discrepancy is likely a combination of the effects of low ecliptic latitude on declination precision and covariance with other measured parameters.

The large timing declination proper motion is also unphysical. If Ter5A is indeed a cluster member, its elliptical orbit about the cluster core would never take it on the measured trajectory. It cannot even be sensibly ejected in this direction. While in principle these results could suggest that Ter5A is not actually a cluster member, this is highly unlikely. The observed positive spin frequency derivative practically guarantees cluster membership.

However, if we instead fit for the position of the pulsar over just a few years of well-sampled, smoothly behaved data at a time, we get results in the RA-direction that are consistent with *Gaia*’s proper motion measurements, as shown in Figure 8. However, the declination results are too ridden with systematic errors to draw any conclusions.

We compare our timing positions to VLA positions in Table 3 and Figure 8. The details of the first two VLA positions are described in Fruchter & Goss (2000) and Urquhart et al. (2020). The last position, from Urquhart et al. (in prep), is obtained by propagating pulsar timing positions and *Gaia* proper motions from the 55000 MJD epoch to 59669 MJD. Continuum images were shifted by matching to 20 timed pulsar positions, though Ter5A was excluded from the frame shift calculation. The new positional uncertainties come from the quadrature sum of the rms associated with the PSR frame shift and the thermal fluctuations in the continuum position fitting. With Ter5A being such a bright source, we are dominated by the PSR frame shift uncertainties.

As a result, we use the SPIGOT timing position and the proper motion measured by *Gaia* (Vasiliev & Baumgardt 2021) for our long-term timing solution. These are the parameters that produced the residuals in Figure 3.

4.6. Comparison with X-Ray Data

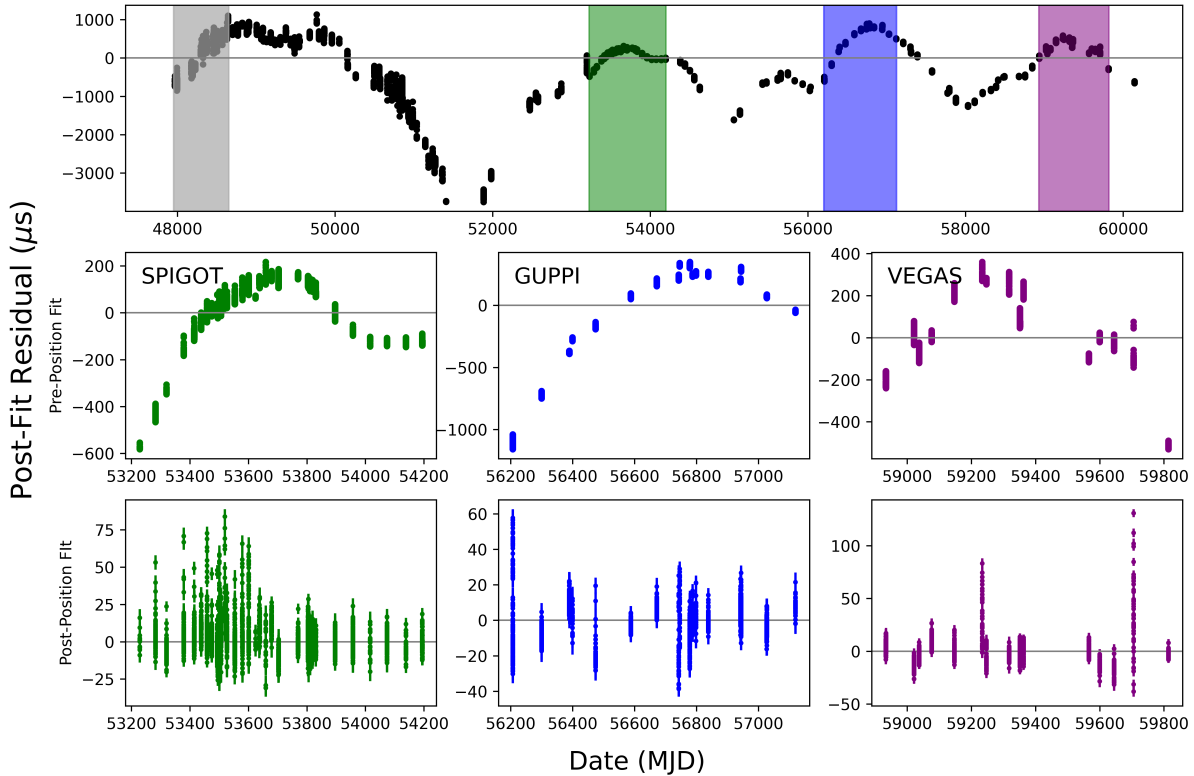


Figure 7. Fitting over a few years of well-sampled data at a time results in positions that are reasonably consistent with *Gaia* proper motion measurements of Terzan 5 as a whole (see Figure 8). The top panel shows our long-term timing solution shown in the third panel of Figure 3, exempting JB data. The green, blue, and purple highlighted regions correspond to the data ranges used to fit for position. They correspond to different GBT backends and are labeled as such. The second row of plots are the highlighted TOAs in the long-term model. The bottom row are those same TOAs fit for frequency and frequency derivatives 1-4, DM, and position. We use only high-precision GBT data for these fits. These positions are reflected in Table 3 and Figure 8. None of the fitted parameters are covariant > 0.8 with position. The gray band corresponds to TOAs used in *Nice & Thorsett (1992)* to measure position, which is also tabulated in Table 3 and plotted in Figure 8.

Ter5A has an associated variable X-ray source, and it is one of the hardest-spectrum and X-ray brightest MSPs in Terzan 5 (*Bogdanov et al. 2021; Bahramian et al. 2020*). This source might indicate intermittent accretion. Notably, Ter5A has been observed to have high- and low- X-ray emission states, with approximately 40% of its X-ray counts measured during two comparatively short observations where it was ~ 9 times brighter than during other observations (*Bogdanov et al. 2021*). In the “high”-flux state, *Bogdanov et al. (2021)* reports an unabsorbed 0.5-8 keV X-ray luminosity of $L_X = 8.6(2.1) \times 10^{31}$ ergs/s, assuming a distance of 5.9 kpc to the cluster. In the “low”-flux, or quiescent state, this luminosity is $L_X < 1.3 \times 10^{31}$ ergs/s with a photon index of 1.5 ± 2.0 (*Bogdanov et al. 2021*), which places it in the redback-black widow overlap region in L_X -photon index space (see Figure 10 of *Urquhart et al.*

(2020)). The quiescent L_X is lower than that of a typical redback, probably due to a lower-than-typical spindown luminosity.

Bogdanov et al. (2021) suggest two possible interpretations of the data: 1) these luminosity spikes are short-lived burst or flare activity indicating two transitions from a radio pulsar state to an accretion disk-dominated state, or 2) flaring of the companion star. The spectral and variability properties suggest intrabinary shock radiation (*Bogdanov et al. 2021*). The observed flaring is inconsistent with observed transitional MSPs, but could be consistent with magnetic activity from the companion’s surface.

We do not have contemporaneous radio observations during the flared activity. However, a comparison of Ter5A’s X-ray quiet days (in which emission is at Chandra’s detection threshold and not much higher) and its

Paper	Method	RA (s)	Dec (")	Epoch (MJD)
Nice & Thorsett (1992)	Timing	02.2534(11)	37.7(5)	48270
This work	Timing	02.25170(3)	37.40(2)	53711
This work	Timing	02.24918(5)	37.81(2)	56663
This work	Timing	02.249(2)	37.7(4)	59374
Fruchter & Goss (2000)	VLA	02.2685(50)	37.23(5)	47892*
Urquhart et al. (2020)	VLA	02.249(50)	37.65(10)	56663*
Urquhart et al. (in prep)	VLA	02.2534(14)	37.85(2)	59669

Table 3. J2000 measured positions of Ter5A represented in Figure 8. Listed positions are the RA value in seconds of arc offset from 17h48m and the declination value in arcseconds offset from $-24^{\circ} 46'$. Note the timing errors are statistical and reported VLA errors are 1σ . The reported uncertainty on the position measured by Fruchter & Goss (2000) does not include the systematic uncertainty from the position of the phase calibrator used or from phase interpolation uncertainties, and hence is potentially underestimated.

*Approximate value

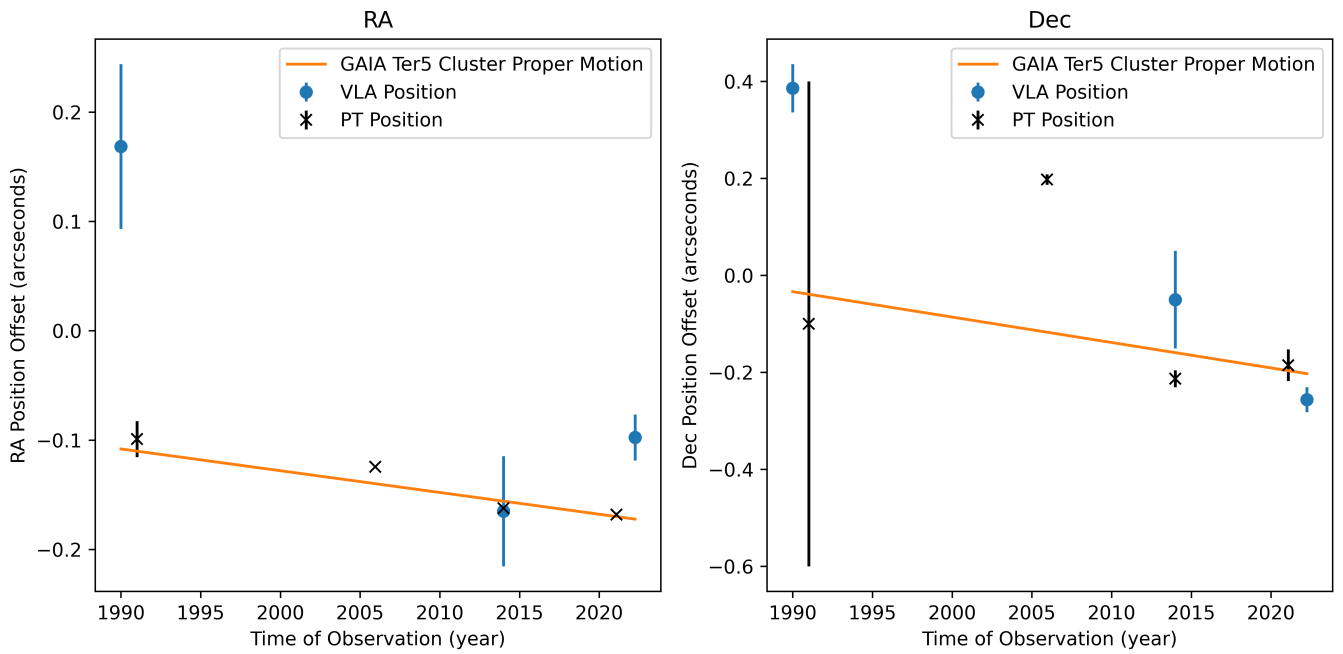


Figure 8. A comparison of pulsar timing and VLA-measured positions of Ter5A with the *Gaia* proper motion of the cluster. The four timing positions are from Nice & Thorsett (1992), and three-year sections of SPIGOT, GUPPI, and VEGAS observations (Figure 7). The VLA positions are from Fruchter & Goss (2000), Urquhart et al. (2020), and Urquhart et al. (in prep), and their error bars are 1σ . Note both right ascension and declination are in units of arcseconds.

flared days with spin frequency residuals and orbital variations is presented in the bottom-most panel of Figure 3. There is no apparent correlation between X-ray activity and changes in either the spin or orbital behavior of the pulsar.

We detect Ter5A in the radio almost every time we observe it. Though there are gaps in our observations, we see very little evidence that Ter5A is radio-silent for any extended period of time and therefore very little evidence that Ter5A spends very much time actively accreting. Even if it were radio-silent for extended pe-

riods of time, that is not in and of itself a smoking gun for transitional behavior. For example, J1653–0158 is a 1.97 ms binary pulsar in a 75-minute orbit that has only been detected in gamma-rays despite 26 radio searches on 8 different observatories over 11 years across all orbital phases and several wavelengths (Nieder et al. 2020). However, J1653–0158’s radio non-detections are attributed to it being eclipsed by ablated material the vast majority of the time. Radio disappearances could simply be due to excess gas in the system and not prolonged accretion-driven X-ray emission.

Ter5A’s behavior is also in stark contrast with the known reback and transitional MSP M28I. M28I also experiences X-ray flux enhancements of 1-2 orders of magnitude when it switches from pulsar- to disk- state (Vurgun et al. 2022). However, in Chandra data, M28I was detected as a pulsar three times from July to September of 2002, as a disk-accreting X-Ray Binary (XRB) on two observations four days apart in August of 2008, and as a pulsar again on three observations from May to November of 2015 (Vurgun et al. 2022). While data are sparse, odds are low that M28I was by chance observed on two consecutive observations as an XRB if its presence in that state is rare. Furthermore, Papitto et al. (2013) reports that M28I’s behavior is consistent with months-long X-ray outbursts. We see no evidence for months-long state changes in Ter5A. M28I is likely stable for much longer periods of time than Ter5A is. We conclude that Ter5A is likely not a transitional MSP. If it is switching between accreting and non-accreting states, these switches are rare and short in duration.

4.7. Energetics

The Applegate model predicts orbital variability due to deformations in the companion star from magnetic activity. It could potentially explain the observed orbital variations if those variations have a clear periodicity.

We investigate if the Applegate model is energetically viable. We assume that the companion star is approximately the radius of its Roche lobe, using Nice et al. (1990)’s value of $0.2 R_\odot$. Consulting a $P-\dot{P}$ diagram, we note the intrinsic spindown of this pulsar is likely of order $\dot{P} \sim 10^{-19} - 10^{-20}$. We assume $\dot{P} = 10^{-19}$ for the following calculations. The energy radiated by the pulsar, or its spindown luminosity, is given by $L_{\text{spin}} = 4\pi^2 I \dot{P} P^{-3}$, where I is taken to be 10^{45} g cm^2 . Assuming isotropic emission, the companion captures an energy of $L_{\text{capt}} = 4.3 \times 10^{31} \text{ ergs/s}$ of this spindown energy, or $0.01 L_\odot$. This energy blows mass off the companion at a maximum rate given by

$$\dot{M}_c = \frac{L_{\text{capt}} \times R_l}{GM_c}, \quad (10)$$

which predicts a value of $1.9 \times 10^{-12} M_\odot/\text{yr}$. This agrees with predictions made by Shaham (1995) and results in an evaporation time much longer than a Hubble time.

The energy available due to tidal heating, denoted L_T for tidal luminosity, is given by

$$L_T = 4 \times 10^{32} \left(\frac{10^{11} \text{ cm}}{a} \right)^2 \frac{M_c}{1.6 M_\odot} \frac{10^8 \text{ yr}}{t_M} \text{ ergs/s} \quad (11)$$

according to Equation 28 of Applegate & Shaham (1994), where t_M is the evaporation time in years of

the companion and a is the separation. This yields $L_T = 1.7 \times 10^{29} \text{ ergs/s}$, or $4.2 \times 10^{-5} L_\odot$.

The Applegate model predicts a change in transported angular momentum ΔJ given by Equation 27 in Applegate (1992):

$$\Delta J = \frac{1}{6\pi} \frac{GM_c^2 a^2}{R_c^3} \Delta P_{\text{orb}}, \quad (12)$$

where R_c is the radius of the companion, here taken to be the Roche lobe radius. The associated energy is given by

$$\Delta E = \Omega_{\text{diff}} \Delta J, \quad (13)$$

where Ω_{diff} is the differential rotation between layers of the star. This is not measurable, but since existing constraints are of order ~ 0.01 of the total orbital angular velocity of the system, we will take the generous assumption that it is 0.1Ω to test the model’s energetic viability. Noting that $\Delta P_{\text{orb}}/\Delta t \sim \dot{P}_{\text{orb}}$ for Δt the length of the dataset, Eqn 13 can be rewritten to express the luminosity predicted by the Applegate model ΔL_A :

$$\Delta L_A = 13 \times 10^{33} \left(\frac{M_c}{M_\odot} \right)^2 \left(\frac{10^{10} \text{ cm}}{R_c} \right)^3 \times \left(\frac{a}{10^{10} \text{ cm}} \right)^2 \left(\frac{\dot{P}_{\text{orb}}}{10^{-9}} \right) \text{ ergs/s}. \quad (14)$$

This yields $\Delta L_A = 3.5 \times 10^{29} \text{ ergs/s}$, or $8.9 \times 10^{-5} L_\odot$. We conclude that the Applegate model is energetically viable - there is more than sufficient spindown energy ($0.01 L_\odot$), and an available tidal heating energy reservoir of the same order of magnitude ($4.2 \times 10^{-5} L_\odot$), to drive these changes.

While energetically viable, we observe no periodicity in the T0 measurements in Figure 5 to suggest that this process is taking place on a timescale even of a few decades. However, it is certainly possible that some other form of energy exchange is occurring between the orbit and the companion.

4.8. Torques

If any of the ablated material falls back on the pulsar, it should torque the pulsar and affect its spin as the second derivative of phase ϕ :

$$\tau = I \frac{d^2 \phi}{dt^2}. \quad (15)$$

This quantity is related to (but not equivalent to) the second derivative of the timing residuals. From Figure 9, it’s apparent that the slope of the first derivative is high around the odd feature at about MJD 51500, so that feature does indeed correspond to some type of torque.

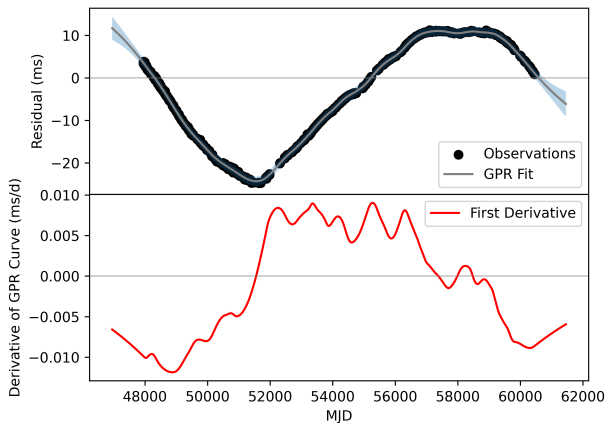


Figure 9. The F0- and F1-subtracted pulse residuals and their GPR fit are plotted in the top panel, and the first derivative of this curve is plotted in the bottom. Note the strong feature around MJD 51500 corresponds to a steep slope in the first derivative plot, which is likely related to a torque on the neutron star.

It is unclear whether this torque is intrinsic (such as internal seismic activity) or extrinsic (such as accretion or the effects of a nearby star), but similar sharp features also appear later in the data.

These sharp turnarounds are inconsistent with glitches, as the pulses after the turnarounds are showing up later, not earlier, as would be expected for the increase in spin frequency following a glitch. These events all show the pulsar slowing down in its rotation. One possible explanation is that gas interacting with the magnetosphere is hindering Ter5A’s rotation, but the mechanism driving these spin features is very unclear.

4.9. Known Systematics

There remain contaminants in the data. In order to limit the number of TOAs and focus on phase connection, much of the radio frequency information available in the original data has been discarded. For an example and analysis of how DM can vary over the course of a single Ter5A observation, see Figure 10 of [Bilous et al. \(2019\)](#). This figure is an analysis of the first observation in the GUPPI panel in Figure 7, and shows a DM change of $\sim 0.6 \text{ pc cm}^{-3}$ in a systematic manner over the course of the observation. This is an example of a day in which DM variations – which we do not account for in our study – prohibit precise measurement of T0. Similar DM-related effects are likely present during most observations, but with smaller amplitudes.

Of the nine redback pulsars with long-term timing solutions published or in preparation ([Thongmeearkom et al. \(2024\)](#), [Corcoran et al, in prep](#)), Ter5A has by

far the most timing noise. Six redbacks show effectively flat timing residuals when fit out to the second frequency derivative, and two show flat residuals when fit to the fourth frequency derivative ([Thongmeearkom et al. \(2024\)](#), [Corcoran et al, in prep](#)), while Ter5A shows systematics at the $\sim 1 \text{ ms}$ level even when fit to the fifth frequency derivative.

5. CONCLUSIONS & FUTURE WORK

We have determined a 34-year duration timing solution for the eclipsing millisecond pulsar Terzan 5A, the longest timing solution for any redback system. We successfully used novel timing methods such as iterative parameter-fitting, employing a continuous binary piecewise model, and using precise binary values to remove the orbital motion of the pulsar and effectively isolate it.

There are strong systematic timing residuals, but they don’t seem to directly correspond to measured orbital variations. The amount of timing noise in this system is far greater than that of standard millisecond pulsar systems and complicates or inhibits many traditional pulsar timing methods, including precision measurements of position and proper motion. This timing noise could be caused by torques on the pulsar due to infalling matter, or by other dynamical effects due to the dense cluster environment. While we successfully phase-connected 34 years of observations, this is too complex a system to to explain all of the residuals in our data with a simple physical model. Systematic effects remain at the 1 ms level.

We measured the orbital decay of the system over time and found it consistent with GR predictions for a companion of mass $0.1 M_{\odot}$, a highly-inclined orbit, and a pulsar of 1.5 to $1.8 M_{\odot}$. Though our measurements are not inconsistent with a higher-mass pulsar for very low effective spin and galactic accelerations, it is unlikely that Ter5A achieved such a mass given its relatively slow spin period. General relativity seems to be the dominant effect in the measured orbital period derivative, which constrains the magnitude of tidal effects in this system to be at most 30% of the observed acceleration, and likely much less.

We could not use long-term timing to determine precise positions or proper motions of the system because over long-term timing baselines timing noise strongly contaminates the timing signals of these parameters. However, measuring position via timing over few-year periods yielded reasonable position measurements consistent with a measured *Gaia* proper motion for Terzan 5.

The power spectral density of Ter5A’s orbital variations is consistent with those of other redback systems, and is roughly power-law in nature, although with a shallower spectrum than some of the other systems. The variations in orbit and sometimes strong changes in spin as measured by pulsar timing do not seem to correlate with measured X-ray emission.

Possible directions for future work include measuring time-variable DMs over the course of all observations, providing insight into Ter5A’s environment. Another is to use our model and all TOAs, including those affected by the eclipse, to examine in greater depth the eclipses themselves. Furthermore, the torque on the pulsar can be calculated and compared to wind-based accretion models as well as the precession of the system predicted in [Nice et al. \(2000\)](#). Investigating the systematics in the spin frequency derivative residuals could reveal more about the source of the timing noise. Are

they from e.g. the companion, internal neutron star processes, cluster dynamics, or infalling gas?

1 The National Radio Astronomy Observatory and Green
2 Bank Observatory are facilities of the U.S. National
3 Science Foundation operated under cooperative agree-
4 ment by Associated Universities, Inc. Murriyang, the
5 Parkes radio telescope, is part of the Australia Telescope
6 National Facility (<https://ror.org/05qajvd42>) which is
7 funded by the Australian Government for operation as
8 a National Facility managed by CSIRO. We acknowl-
9 edge the Wiradjuri people as the Traditional Own-
10 ers of the Observatory site. SMR is a CIFAR Fellow
11 and is supported by the NSF Physics Frontiers Cen-
12 ter award 2020265. DJN is also supported by NSF
13 award 2020265. JS acknowledges support from NASA
14 grant 80NSSC21K0628, NSF grant AST-2205550, and
15 the Packard Foundation.

REFERENCES

- Abbate, F., Possenti, A., Ridolfi, A., et al. 2018, *MNRAS*, 481, 627, doi: [10.1093/mnras/sty2298](https://doi.org/10.1093/mnras/sty2298)
- Applegate, J. H. 1992, *ApJ*, 385, 621, doi: [10.1086/170967](https://doi.org/10.1086/170967)
- Applegate, J. H., & Shaham, J. 1994, *ApJ*, 436, 312, doi: [10.1086/174906](https://doi.org/10.1086/174906)
- Archibald, A. M., Kaspi, V. M., Hessels, J. W. T., et al. 2013, arXiv e-prints, arXiv:1311.5161, doi: [10.48550/arXiv.1311.5161](https://doi.org/10.48550/arXiv.1311.5161)
- Bahramian, A., Strader, J., Miller-Jones, J. C. A., et al. 2020, *ApJ*, 901, 57, doi: [10.3847/1538-4357/aba51d](https://doi.org/10.3847/1538-4357/aba51d)
- Bilous, A. V., Ransom, S. M., & Demorest, P. 2019, *ApJ*, 877, 125, doi: [10.3847/1538-4357/ab16dd](https://doi.org/10.3847/1538-4357/ab16dd)
- Bilous, A. V., Ransom, S. M., & Nice, D. J. 2011, in *American Institute of Physics Conference Series*, Vol. 1357, *Radio Pulsars: An Astrophysical Key to Unlock the Secrets of the Universe*, ed. M. Burgay, N. D’Amico, P. Esposito, A. Pellizzoni, & A. Possenti (AIP), 140–141, doi: [10.1063/1.3615100](https://doi.org/10.1063/1.3615100)
- Bogdanov, S., Bahramian, A., Heinke, C. O., et al. 2021, *ApJ*, 912, 124, doi: [10.3847/1538-4357/abee78](https://doi.org/10.3847/1538-4357/abee78)
- Chen, H.-L., Chen, X., Tauris, T. M., & Han, Z. 2013, *The Astrophysical Journal*, 775, 27, doi: [10.1088/0004-637x/775/1/27](https://doi.org/10.1088/0004-637x/775/1/27)
- Clark, C. J., Nieder, L., Voisin, G., et al. 2021, *MNRAS*, 502, 915, doi: [10.1093/mnras/staa3484](https://doi.org/10.1093/mnras/staa3484)
- Clark, G. W. 1975, *ApJL*, 199, L143, doi: [10.1086/181869](https://doi.org/10.1086/181869)
- De Vito, M. A., Benvenuto, O. G., & Horvath, J. E. 2020, *MNRAS*, 493, 2171, doi: [10.1093/mnras/staa395](https://doi.org/10.1093/mnras/staa395)
- Deneva, J. S., Ray, P. S., Camilo, F., et al. 2016, *ApJ*, 823, 105, doi: [10.3847/0004-637X/823/2/105](https://doi.org/10.3847/0004-637X/823/2/105)
- DuPlain, R., Ransom, S., Demorest, P., et al. 2008, in *Society of Photo-Optical Instrumentation Engineers (SPIE) Conference Series*, Vol. 7019, *Advanced Software and Control for Astronomy II*, ed. A. Bridger & N. M. Radziwill, 70191D, doi: [10.1117/12.790003](https://doi.org/10.1117/12.790003)
- EPTA Collaboration and InPTA Collaboration, Antoniadis, J., Arumugam, P., et al. 2023, *A&A*, 678, A50, doi: [10.1051/0004-6361/202346844](https://doi.org/10.1051/0004-6361/202346844)
- Freire, P. C. C., & Wex, N. 2024, *Living Reviews in Relativity*, 27, 5, doi: [10.1007/s41114-024-00051-y](https://doi.org/10.1007/s41114-024-00051-y)
- Fruchter, A. S., & Goss, W. M. 2000, *ApJ*, 536, 865, doi: [10.1086/308948](https://doi.org/10.1086/308948)
- Gaia Collaboration, Brown, A. G. A., Vallenari, A., et al. 2021, *A&A*, 649, A1, doi: [10.1051/0004-6361/202039657](https://doi.org/10.1051/0004-6361/202039657)
- Ghosh, A., Bhattacharyya, B., Lyne, A., et al. 2024, *ApJ*, 965, 64, doi: [10.3847/1538-4357/ad31ab](https://doi.org/10.3847/1538-4357/ad31ab)
- Ginzburg, S., & Quataert, E. 2021, *MNRAS*, 500, 1592, doi: [10.1093/mnras/staa3358](https://doi.org/10.1093/mnras/staa3358)
- Hessels, J. W. T., Ransom, S. M., Stairs, I. H., et al. 2006, *Science*, 311, 1901, doi: [10.1126/science.1123430](https://doi.org/10.1126/science.1123430)
- Kaplan, D. L., Escoffier, R. P., Lacasse, R. J., et al. 2005, *PASP*, 117, 643, doi: [10.1086/430368](https://doi.org/10.1086/430368)
- Katz, J. I. 1975, *Nature*, 253, 698, doi: [10.1038/253698a0](https://doi.org/10.1038/253698a0)
- Lattimer, J. M. 2021, *Annual Review of Nuclear and Particle Science*, 71, 433, doi: [10.1146/annurev-nucl-102419-124827](https://doi.org/10.1146/annurev-nucl-102419-124827)

- Li, D., Bilous, A., Ransom, S., Main, R., & Yang, Y.-P. 2023, *Nature*, 618, 484, doi: [10.1038/s41586-023-05983-z](https://doi.org/10.1038/s41586-023-05983-z)
- Luo, J., Ransom, S., Demorest, P., et al. 2021, *ApJ*, 911, 45, doi: [10.3847/1538-4357/abe62f](https://doi.org/10.3847/1538-4357/abe62f)
- Lyne, A. G., Biggs, J. D., Harrison, P. A., & Bailes, M. 1993, *Nature*, 361, 47, doi: [10.1038/361047a0](https://doi.org/10.1038/361047a0)
- Lyne, A. G., Manchester, R. N., D'Amico, N., et al. 1990, *Nature*, 347, 650, doi: [10.1038/347650a0](https://doi.org/10.1038/347650a0)
- Martsen, A. R., Ransom, S. M., DeCesar, M. E., et al. 2022, *ApJ*, 941, 22, doi: [10.3847/1538-4357/aca156](https://doi.org/10.3847/1538-4357/aca156)
- Miraval Zanon, A., Burgay, M., Possenti, A., & Ridolfi, A. 2018, in *Journal of Physics Conference Series*, Vol. 956, *Journal of Physics Conference Series (IOP)*, 012004, doi: [10.1088/1742-6596/956/1/012004](https://doi.org/10.1088/1742-6596/956/1/012004)
- Nice, D., Thorsett, S., Taylor, J., & Fruchter, A. 1990, *The Astrophysical Journal Letters*, 361, L61, doi: [10.1086/185827](https://doi.org/10.1086/185827)
- Nice, D. J., Arzoumanian, Z., & Thorsett, S. E. 2000, in *Astronomical Society of the Pacific Conference Series*, Vol. 202, *IAU Colloq. 177: Pulsar Astronomy - 2000 and Beyond*, ed. M. Kramer, N. Wex, & R. Wielebinski, 67, doi: [10.48550/arXiv.astro-ph/9911211](https://doi.org/10.48550/arXiv.astro-ph/9911211)
- Nice, D. J., & Thorsett, S. E. 1992, *ApJ*, 397, 249, doi: [10.1086/171784](https://doi.org/10.1086/171784)
- Nieder, L., Clark, C. J., Kandel, D., et al. 2020, *ApJL*, 902, L46, doi: [10.3847/2041-8213/abb0c2](https://doi.org/10.3847/2041-8213/abb0c2)
- Özel, F., & Freire, P. 2016, *ARA&A*, 54, 401, doi: [10.1146/annurev-astro-081915-023322](https://doi.org/10.1146/annurev-astro-081915-023322)
- Padmanabh, P. V., Ransom, S. M., Freire, P. C. C., et al. 2024, *arXiv e-prints*, arXiv:2403.17799, doi: [10.48550/arXiv.2403.17799](https://doi.org/10.48550/arXiv.2403.17799)
- Papitto, A., Ferrigno, C., Bozzo, E., et al. 2013, *Nature*, 501, 517, doi: [10.1038/nature12470](https://doi.org/10.1038/nature12470)
- Pathak, D., & Bagchi, M. 2018, *ApJ*, 868, 123, doi: [10.3847/1538-4357/aae9d9](https://doi.org/10.3847/1538-4357/aae9d9)
- Patruno, A., Archibald, A. M., Hessels, J. W. T., et al. 2014, *ApJL*, 781, L3, doi: [10.1088/2041-8205/781/1/L3](https://doi.org/10.1088/2041-8205/781/1/L3)
- Peters, P. C., & Mathews, J. 1963, *Physical Review*, 131, 435, doi: [10.1103/PhysRev.131.435](https://doi.org/10.1103/PhysRev.131.435)
- Phinney, E. S. 1993, in *Astronomical Society of the Pacific Conference Series*, Vol. 50, *Structure and Dynamics of Globular Clusters*, ed. S. G. Djorgovski & G. Meylan, 141
- Polzin, E. J., Breton, R. P., Stappers, B. W., & LOFAR PWG. 2018, in *Pulsar Astrophysics the Next Fifty Years*, ed. P. Weltevrede, B. B. P. Perera, L. L. Preston, & S. Sanidas, Vol. 337, 396–397, doi: [10.1017/S1743921317009115](https://doi.org/10.1017/S1743921317009115)
- Prager, B. J., Ransom, S. M., Freire, P. C. C., et al. 2017, *ApJ*, 845, 148, doi: [10.3847/1538-4357/aa7ed7](https://doi.org/10.3847/1538-4357/aa7ed7)
- Prestage, R. M., Bloss, M., Brandt, J., et al. 2015, in 2015 *URSI-USNC Radio Science Meeting*, 4, doi: [10.1109/USNC-URSI.2015.7303578](https://doi.org/10.1109/USNC-URSI.2015.7303578)
- Ransom, S. 2011, *PRESTO: Pulsar Exploration and Search TOolkit*, *Astrophysics Source Code Library*, record ascl:1107.017
- Ransom, S. M. 2001, PhD thesis, Harvard University, Massachusetts
- Ransom, S. M., Hessels, J. W. T., Stairs, I. H., et al. 2005, *Science*, 307, 892, doi: [10.1126/science.1108632](https://doi.org/10.1126/science.1108632)
- Ridolfi, A., Freire, P. C. C., Torne, P., et al. 2016, *MNRAS*, 462, 2918, doi: [10.1093/mnras/stw1850](https://doi.org/10.1093/mnras/stw1850)
- Roberts, M. S. E. 2013, in *Neutron Stars and Pulsars: Challenges and Opportunities after 80 years*, ed. J. van Leeuwen, Vol. 291, 127–132, doi: [10.1017/S174392131202337X](https://doi.org/10.1017/S174392131202337X)
- Shaham, J. 1995, in *Astronomical Society of the Pacific Conference Series*, Vol. 72, *Millisecond Pulsars. A Decade of Surprise*, ed. A. S. Fruchter, M. Tavani, & D. C. Backer, 126
- Shapiro, S. L., & Teukolsky, S. A. 1983, *Black holes, white dwarfs and neutron stars. The physics of compact objects* (Wiley-VCH), doi: [10.1002/9783527617661](https://doi.org/10.1002/9783527617661)
- Stappers, B. W., Archibald, A. M., Hessels, J. W. T., et al. 2014, *ApJ*, 790, 39, doi: [10.1088/0004-637X/790/1/39](https://doi.org/10.1088/0004-637X/790/1/39)
- Strader, J., Swihart, S., Chomiuk, L., et al. 2019, *ApJ*, 872, 42, doi: [10.3847/1538-4357/aafbaa](https://doi.org/10.3847/1538-4357/aafbaa)
- Susobhanan, A., Gopakumar, A., Joshi, B. C., & Kumar, R. 2018, *MNRAS*, 480, 5260, doi: [10.1093/mnras/sty2177](https://doi.org/10.1093/mnras/sty2177)
- Susobhanan, A., Kaplan, D., Archibald, A., et al. 2024, *arXiv e-prints*, arXiv:2405.01977, doi: [10.48550/arXiv.2405.01977](https://doi.org/10.48550/arXiv.2405.01977)
- Tavani, M., & Brookshaw, L. 1993, *A&A*, 267, L1
- Taylor, D. J., Mason, A. C., Schiavon, R. P., et al. 2022, *MNRAS*, 513, 3429, doi: [10.1093/mnras/stac968](https://doi.org/10.1093/mnras/stac968)
- Taylor, J. H., & Weisberg, J. M. 1982, *ApJ*, 253, 908, doi: [10.1086/159690](https://doi.org/10.1086/159690)
- Thongmearkom, T., Clark, C. J., Breton, R. P., et al. 2024, *MNRAS*, 530, 4676, doi: [10.1093/mnras/stae787](https://doi.org/10.1093/mnras/stae787)
- Thorsett, S. E., & Nice, D. J. 1991, *Nature*, 353, 731, doi: [10.1038/353731a0](https://doi.org/10.1038/353731a0)
- Urquhart, R., Bahramian, A., Strader, J., et al. 2020, *ApJ*, 904, 147, doi: [10.3847/1538-4357/abb6fc](https://doi.org/10.3847/1538-4357/abb6fc)
- Vasiliev, E., & Baumgardt, H. 2021, *MNRAS*, 505, 5978, doi: [10.1093/mnras/stab1475](https://doi.org/10.1093/mnras/stab1475)
- Vurgun, E., Linares, M., Ransom, S., et al. 2022, *ApJ*, 941, 76, doi: [10.3847/1538-4357/ac9ea0](https://doi.org/10.3847/1538-4357/ac9ea0)
- You, X. P., Manchester, R. N., Coles, W. A., Hobbs, G. B., & Shannon, R. 2018, *ApJ*, 867, 22, doi: [10.3847/1538-4357/aadee0](https://doi.org/10.3847/1538-4357/aadee0)

Table 4. Our final measurements for T_0 for Ter5A.

Group #	T_0 [MJD]	Group #	T_0 [MJD]	Group #	T_0 [MJD]
1	47967.5211462(25)	49	51142.691189(53)	97	55653.468991(86)
2	47992.8625959(33)	50	51184.7504350(17)	98	55743.336581410(36)
3	48182.8856352(22)	51	51236.9462491(14)	99	55829.951378509(43)
4	48225.85262672(85)	52	51265.918711(13)	100	55931.61975729(14)
5	48268.6683358(10)	53	51383.2458160(22)	101	56027.76596080(11)
6	48301.0448706(16)	54	51884.0231145(21)	102	56206.895965627(46)
7	48324.9490412(36)	55	51979.94239029(41)	103	56299.638095659(43)
8	48366.4031143(44)	56	52468.01112700(41)	104	56389.35438867(24)
9	48457.5566862(48)	57	52546.38049423(66)	105	56399.33967526(20)
10	48501.960954(85)	58	52573.91567960(43)	106	56474.229326535(27)
11	48568.832117(25)	59	52826.19547329(49)	107	56587.849792656(53)
12	48633.0556662(72)	60	52869.994569(90)	108	56671.590041286(69)
13	48698.413910(15)	61	53193.3060992(25)	109	56743.907724038(85)
14	48759.2333977(51)	62	53228.02763380(11)	110	56782.714179(50)
15	48821.1875594(31)	63	53281.887669276(59)	111	56798.145987630(65)
16	48877.9221511(45)	64	53319.78637056(16)	112	56838.162781910(43)
17	48901.9019577(25)	65	53378.639047620(88)	113	56942.857002491(48)
18	49004.705062(14)	66	53414.495304212(86)	114	57026.67289664(98)
19	49004.7050624(89)	67	53438.399476352(89)	115	57119.339385812(59)
20	49061.4396263(21)	68	53466.31289481(14)	116	57209.131320225(42)
21	49086.8567026(15)	69	53503.30384691(29)	117	57302.856855201(45)
22	49128.3107882(70)	70	53522.820545107(97)	118	57387.656147661(46)
23	49184.591495(70)	71	53553.15463624(13)	119	57573.140418710(33)
24	49236.938586(23)	72	53579.10125297(22)	120	57769.5933781(24)
25	49303.8097748(13)	73	53600.96297964(13)	121	57791.6064045(17)
26	49372.1182084(61)	74	53631.0701342(68)	122	57875.271003766(80)
27	49434.9044942(17)	75	53659.059202373(62)	123	58030.87505377(30)
28	49480.7460397(19)	76	53678.878476315(45)	124	58113.6318991(62)
29	49544.6670191(14)	77	53702.782646032(46)	125	58215.30028134(11)
30	49676.2912430(14)	78	53769.57816795(35)	126	58320.070144442(90)
31	49781.5906512(15)	79	53811.4861145(21)	127	58384.898861061(76)
32	49858.7496867(23)	80	53830.47328809(96)	128	58412.812278032(51)
33	49958.5269046(47)	81	53896.4366994(11)	129	58486.113361403(61)
34	50052.78196093(90)	82	53956.95359396(65)	130	58676.13639872(59)
35	50157.930063(43)	83	54015.42804086(67)	131	58753.9006012(15)
36	50261.3383028(15)	84	54073.448609(35)	132	58844.675942632(60)
37	50492.9667102(12)	85	54138.42861983(88)	133	58933.408827089(39)
38	50564.3009975(60)	86	54194.48239060(60)	134	59029.101158831(54)
39	50663.5486979(17)	87	54379.9666671(11)	135	59076.001752235(65)
40	50714.458531(35)	88	54437.98723631(11)	136	59146.80651910(22)
41	50730.8737453(16)	89	54500.546569301(67)	137	59240.00252734(85)
42	50782.3130975(39)	90	54556.37339788(13)	138	59317.388495254(21)
43	50818.1693568(61)	91	54626.270407(31)	139	59356.724475713(72)
44	50852.21011121(87)	92	55058.966185250(56)	140	59565.734689747(72)
45	50925.889426(41)	93	55136.806040349(63)	141	59599.69979484(13)
46	50938.2197420(23)	94	55423.050929003(71)	142	59644.4066483(12)
47	50979.7494554(32)	95	55472.901718495(35)	143	59705.30176143(95)
48	51035.9545259(15)	96	55614.43559669(62)	144	59814.0808785(20)

Table 5. Timing Parameters

Parameter	Simple F2	F5
Pulsar Name	PSR J1748–2446A	–
Timing Parameters		
Right Ascension (RA, J2000) ...	17 ^h 48 ^m 02 ^s .24918(4)	–
Declination (DEC, J2000)	–24° 46′ 37″.81(2)	–
Proper Motion ^a in RA (mas yr ^{–1}) .	–2.0	–
Proper Motion ^a in DEC (mas yr ^{–1})	–5.2	–
Position Epoch (POSEPOCH, MJD)	56663.0	–
Pulsar Spin Period (ms)	11.5631483824071(6)	–
Pulsar Spin Frequency (Hz)	86.481636914861(5)	86.48163691333(7)
Spin Frequency Derivative (Hz s ^{–1})	1.31969(9) × 10 ^{–16}	1.446(8) × 10 ^{–16}
Frequency 2nd Derivative (Hz s ^{–2})	1.433(1) × 10 ^{–25}	2.29(6) × 10 ^{–25}
Frequency 3rd Derivative (Hz s ^{–3})	–	–1.4(1) × 10 ^{–33}
Frequency 4th Derivative (Hz s ^{–4})	–	–4.2(4) × 10 ^{–42}
Frequency 5th Derivative (Hz s ^{–5})	–	9.3(8) × 10 ^{–50}
Reference Epoch (PEPOCH, MJD)	54221.719971	–
Dispersion Measure (DM, pc cm ^{–3})	242.36(2)	–
DM Derivative (pc cm ^{–3} yr ^{–1}) ...	0.014(2)	–
Span of Timing Data (MJD)	47952–60491	–
Orbital Parameters		
Orbital Period (days)	0.07564611426(5)	–
Orbital Period Derivative	–2.5(3) × 10 ^{–13}	–
Projected Semi-Major Axis (lt-s) .	0.119624(2)	–
Ref. Epoch of Periastron (<i>T</i> ₀ , MJD)	54015.8062583(1)	–
Orbital Eccentricity	0	–
Longitude of Periastron, (<i>ω</i> , deg) .	0	–
Derived Parameters		
Mass Function (<i>M</i> _⊙)	0.00032119(2)	–
Min Companion Mass (<i>M</i> _⊙)	≥ 0.089	–

^aThe proper motion was fixed at the GAIA proper motion of the cluster.

NOTE—Numbers in parentheses represent 1- σ uncertainties in the last digit as determined by `TEMPO`, `PINT`, or via standard error propagation, although many of the timing parameters are dominated by systematic errors. The timing solutions used the DE440 Solar System Ephemeris and times are all in Barycentric Dynamical Time (TDB), referenced to TT(BIPM2021). Minimum companion mass was calculated assuming a pulsar mass of 1.4 *M*_⊙.